Supporting Information

Ribbon-like Nickel Cobaltite with Layer-by-layer Assembled Ordered Nano-crystallites for Next Generation All-Solid-State Hybrid Supercapatteries

Siddhant Srivastav[a], Mahesh Kumar Paliwal[a] and Sumanta Kumar Meher[a]*

[a]Materials Electrochemistry & Energy Storage Laboratory, Department of Chemistry, Malaviya National Institute of Technology Jaipur, Rajasthan 302017, India

Email*: skmeher.chy@mnit.ac.in

Physicochemical Analyses: Physicochemical Analyses: The powder X-ray diffraction (PXRD) of the electrode material was measured in a PANalytical X-ray diffractometer, operating at a scan rate of 0.01° s^{-1}, using a Cu K_α (λ= 0.15408 nm) radiation. The Scherrer equation *i.e.* $D = K\lambda/\beta\cos\theta$ (D = crystallite size in nm; K (spherical shape factor) =0.89; and β = full width at half-maximum height (FWHM) of the maximum intense diffraction peak) was used to estimate the average crystallite size of the material. The FT-Raman measurement was performed in a He-Cd laser equipped AIRIX STR 500 confocal Raman spectrometer, operating with an excitation wavelength and a spectral resolution of 532 nm and 1 cm^{-1}, respectively. The X-ray photoelectron spectroscopy (XPS) measurements were carried out in a SCIENT OMICRON MULTIPROBE MXPS spectrometer, equipped with an XM 1000 X-Ray monochromator and a HIS 13 VUV source for UPS measurements. The XPS spectra were recorded by using Al Kα (1486.6 eV) as the radiation source with a resolution of 0.8 eV. The field emission scanning electron microscopy (FESEM) measurements were carried out in a field emission gun equipped FEI-Nova Nano SEM 450 microscope. The electrode material was uniformly spread over a conductive carbon tape before mounting it inside the instrument for FESEM analyses. The high-resolution transmission

electron microscopy (HRTEM) measurements were carried out in an FEITecnai G^2 20 S-Twin microscope, operating at an accelerating voltage of 200 kV.

Based on the microstructural physiognomies, the plausible formation mechanism of ribbon-like $NiCo_2O_4$ is proposed in Scheme S1. Inclusively, the low crystallinity and high polycrystallinity of $NiCo_2O_4$ is ascribed to the controlled-rate precursor formation and restricted crystal growth, which are collectively due to the slow decomposition rate of disodium tartrate and effective crystallite capping by NH_4F.[S1,S2] Notably, the in situ decomposition of disodium tartrate is a kinetically slow process under the adopted reaction condition.[S3] Regarding the plausible formation mechanism, at first, the Ni^{2+} and Co^{2+} ions react with $C_4H_4O_6^{2-}$ (decomposed product of disodium tartrate, as given in reaction set 1) to form the corresponding nascent crystallites of metal-tartrate complex ($NiCo_2(C_4H_4O_6)_3 \cdot nH_2O$), which then undergo active capping by NH_4F, leading to restricted three-dimensional growth of the crystallites.[S4] The NH_4F also controllably decrease the pH of the reaction medium, which further slows down the precipitation/complexation process.[S4,S5] The lowly-crystalline capped-crystallites then undergo regulated Ostwald ripening, coalescence and lateral arrangement to form rod-like microstructure.[S6] The arranged rod-like crystallites then undergo Van der Waals force induced multiple layer-by-layer assembling to form ribbon-like microstructure of $NiCo_2(C_4H_4O_6)_3 \cdot nH_2O$. It should be noted that, the classical arrangement of crystallites followed by the layer-by-layer assembling come off in order to minimize the overall surface energy of the material.[S7,S8] Many ribbon-like microstructures, each composed of crystallite layers then undergo organizational rearrangement to form the overall mesostructure of the precursor material. The precursor on high temperature thermal treatment undergoes chemical decomposition to form ribbon-like $NiCo_2O_4$, with the release of $CO_2\uparrow$ and H_2O.[S9] The release of

gas constituents during the thermal decomposition of mesostructured precursor material leads to generation of additional intrinsic porosity in the ribbon-like $NiCo_2O_4$.[S10]

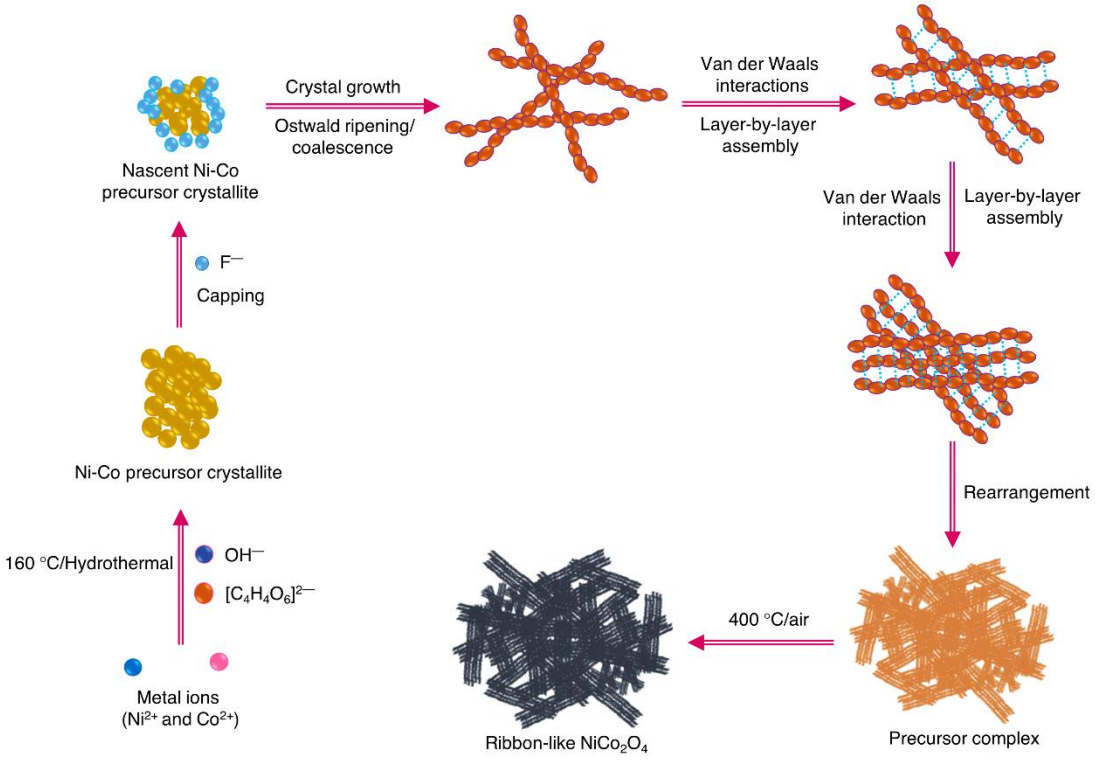

Scheme S1. Plausible mechanism for the growth of ribbon-like $NiCo_2O_4$.

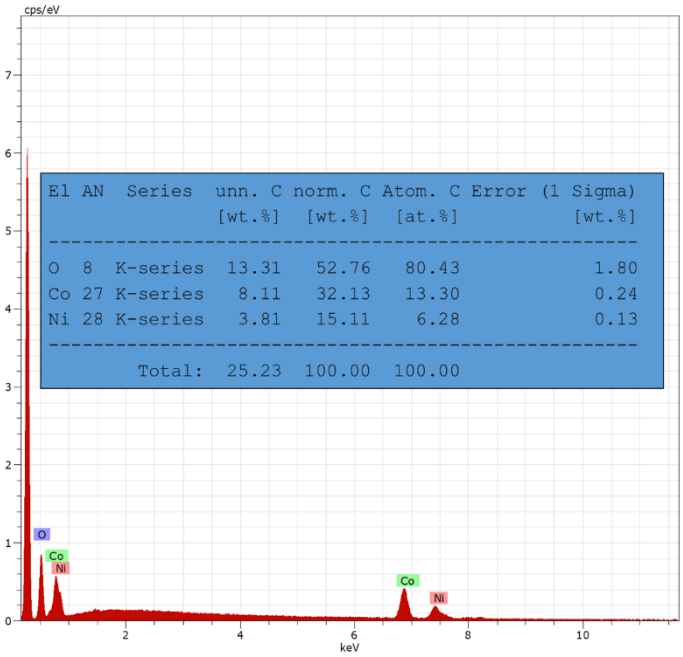

Figure S1. (A) Energy dispersive X-ray Spectroscopy image of ribbon-like $NiCo_2O_4$ showing atomic percentage of Ni, Co and O in the sample

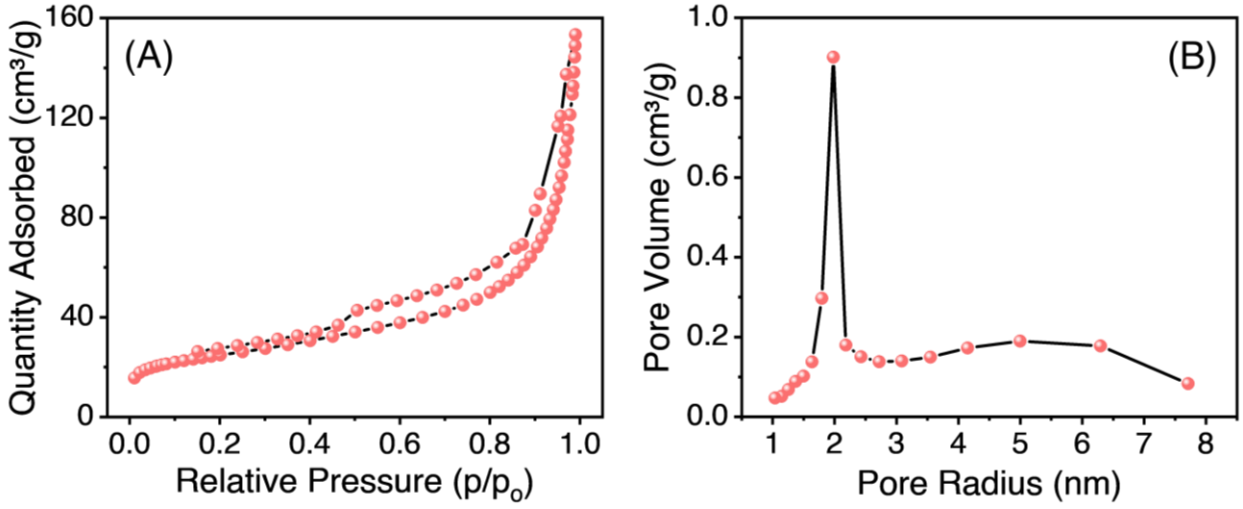

Figure S2. (A) N_2 adsorption-desorption isotherm of ribbon-like $NiCo_2O_4$; and (B) BJH pore size distribution profile of ribbon-like $NiCo_2O_4$.

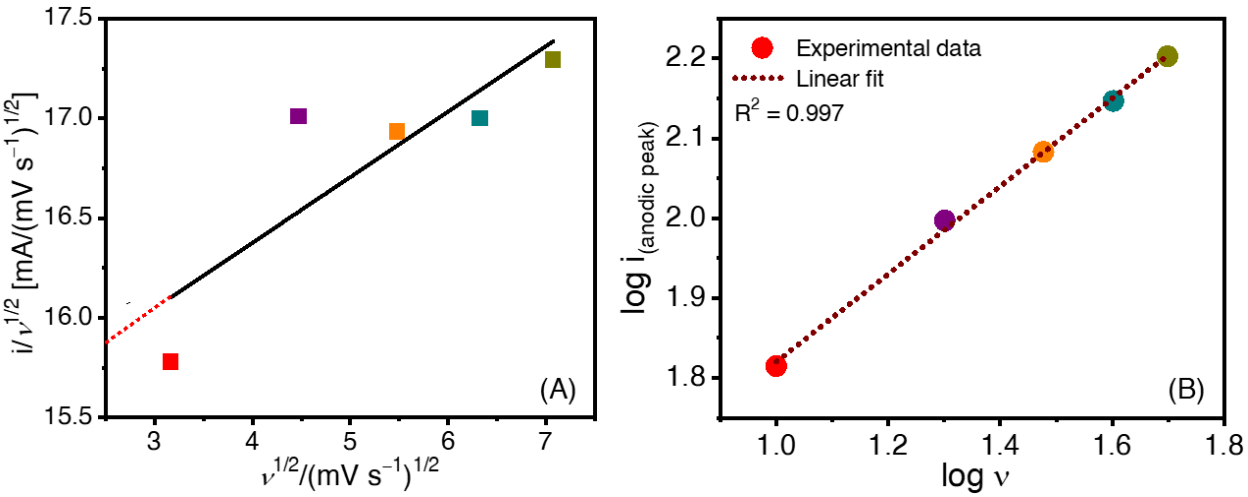

Figure S3. (A) Linear fitted $i/\nu^{1/2}$ vs. $\nu^{1/2}$ plot; and (B) linear fitted *log i* vs. *log v* plot at various scan rates of 10 to 50 mV s^{-1} for ribbon-like $NiCo_2O_4$.

Table S1. Comparison of BET surface area, pore volume and mean pore size of ribbon-like $NiCo_2O_4$ with reported $NiCo_2O_4$ based materials.

Sl. No.	Electrode Material	BET Surface Area (m^2 g^{-1})	Pore Volume (cm^3 g^{-1})	Mean pore size/diameter (nm)	Reference No.
1	$NiCo_2O_4$/NiO/Co_3O_4 nanoflowers	30.84	0.06	7.28	s11
2	$NiCo_2O_4$/NiO structure sphere	34.2	-	2.4	s12
3	$NiCo_2O_4$ hierarchical superstructure	36.7	0.116	-	s13
4	Hierarchical $NiCo_2O_4$/Ni_2P	38.22	-	3.2	s14
5	Chain-like $NiCo_2O_4$ nanowires	42.03	-	10.4	s15
6	$NiCo_2O_4$ nanorods	65.73	0.2	-	s16
7	$NiCo_2O_4$ nanosheets@HfC nanowires	78	-	4.33	s17
8	Ni@$NiCo_2O_4$ core/shell composite	81.2	0.4	-	s18
9	CC/$NiCo_2O_4$-N@NiO	81.3	-	4	s19
10	Mesoporous $NiCo_2O_4$ coated nickel wire	87.4	-	2.73	s20
11	Ribbon-like $NiCo_2O_4$	89	0.37	2.1	This Work

Table S2. Comparison of *specific capacity*, R_{ct} and *EIS* values (derived from electrochemical measurements in 3-electrode setup) for ribbon-like $NiCo_2O_4$ with reported $NiCo_2O_4$ based electrode materials.

Sl. No.	Electrode Material	Specific Capacitance @ Current Density (voltage window)	Specific Capacity @ Current Density (voltage window)	Charge Transfer Resistance (R_{ct})/Equivalent Series Resistance (ESR)	Reference No.
1	$ZnWO_4$ nanoflakes decorated $NiCo_2O_4$ nanoneedle arrays	593 F g^{-1}@ 0.5 A g^{-1} (0.45 V)	296.5 C g^{-1} @ 0.5 A g^{-1} (0.45 V)	-	s21
2	Ni@$NiCo_2O_4$ core/shell composite	597 F g^{-1} @ 1 A g^{-1} (0.5 V)	298.5 C g^{-1} @ 1 A g^{-1} (0.5 V)	0.19 Ω /1.9 Ω	s18
3	Urchin Shaped $NiCo_2O_4$	615 F g^{-1}@ 2 A g^{-1} (0.8 V)	492 C g^{-1} @ 2 A g^{-1} (0.8 V)	0.33 Ω /1.48Ω	s22
4	Urchin and sheaf-like $NiCo_2O_4$ nanostructures	636 F g^{-1} @ 0.5 A g^{-1} (0.45 V)	286.2 C g^{-1} @ 0.5 A g^{-1} (0.45 V)	-	s23
5	$NiCo_2O_4$ hierarchical superstructure	697.8 F g^{-1} @ 1 A g^{-1} (0.5 V)	348.9 C g^{-1} @ 1 A g^{-1} (0.5 V)	-	s13
6	$NiCo_2O_4$ thin film	752 F g^{-1} @ 5mA cm^{-2} (0.5 V)	376 C g^{-1} @ 5mA cm^{-2} (0.5 V)	12.38 Ω /-	s24
7	$NiCo_2O_4$-graphene	845 F g^{-1} @ 1 A g^{-1} (0.5 V)	422.5 C g^{-1} @ 1 A g^{-1} (0.5 V)		s25
8	$NiCo_2O_4$@PANI nanorod arrays	901 F g^{-1} @ 0.25 A g^{-1} (0.8 V)	720.8 C g^{-1} @ 0.25 A g^{-1} (0.8 V)	0.46 Ω / 1.08 Ω	s26
9	$NiCo_2O_4$ nanosheets	1137.5 F g^{-1} @ 5 A g^{-1} (0.4 V)	552.12 C g^{-1} @ 5 A g^{-1} (0.4 V)	0.9 Ω / -	s27
10	Carbon nano-fiberic coated with ambutan-like $NiCo_2O_4$	1152 F g^{-1} @ 1 mA cm^{-2} (0.5 V)	576 C g^{-1} @ 1 mA cm^{-2} (0.5 V)	-	s28
11	Chain-like $NiCo_2O_4$ nanowires	1284 F g^{-1} @ 2 A g^{-1} (0.43 V)	552.12 C g^{-1} @ 2 A g^{-1} (0.43 V)	-	s15

12	Scoparia-like $Ni_{0.3}Co_{2.7}O_4$ Nanostructures	1423 F g^{-1} @ 1 A g^{-1} (0.5 V)	711.5 F g^{-1} @ 1 A g^{-1} (0.5 V)	-	s29
13	Hexagonal $NiCo_2O_4$	1525 F g^{-1} @ 1 A g^{-1} (0.4 V)	610 C g^{-1} @ 1 A g^{-1} (0.4 V)	0.76 Ω / -	s30
14	Hierarchical NiO@$NiCo_2O_4$ core-shell nanosheet arrays	1623.6 F g^{-1} @ 2 A g^{-1} (0.4 V)	649.2 C g^{-1} @ 2 A g^{-1} (0.4 V)	-	s31
15	rGO/ $Ni_{0.3}Co_{2.7}O_4$	1624 F g^{-1} @ 2A g^{-1} (0.5 V)	812 C g^{-1} @ 2 A g^{-1} (0.5 V)	-	s32
16	$NiCo_2O_4$ nanowires	1696 F g^{-1} @ 1 A g^{-1} (0.4 V)	678.4 C g^{-1} @ 1 A g^{-1} (0.4 V)	-	s33
17	$NiCo_2O_4$@polyaniline nanotubes	1801.25 F g^{-1} @ 1 A g^{-1} (0.4 V)	720.5 C g^{-1} @ 1 A g^{-1} (0.4 V)	0.36 Ω / -	s34
18	Carnations-like Mn_3O_4@$NiCo_2O_4$@NiO	1905 F g^{-1} @ 1 A g^{-1} (0.5 V)	952 C g^{-1} @ 1 A g^{-1} (0.5 V)	-	s35
19	Ribbon-like $NiCo_2O_4$	2408 F g^{-1} @ 2 A g^{-1} (0.4 V)	963 C g^{-1} @ 2 A g^{-1} (0.55V)	0.31 Ω / 0.58 Ω	This Work

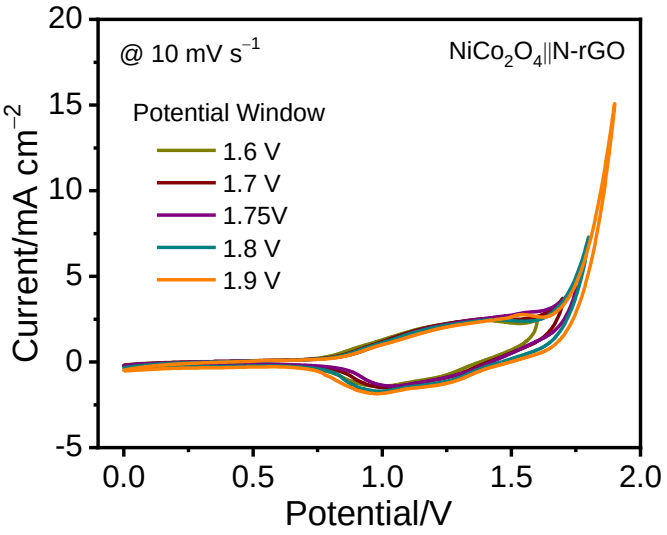

Figure S4. CV plots for $NiCo_2O_4$||N-rGO supercapattery device at different working potential windows.

Table S3. Comparison of *power density*, *energy density* and *cyclic stability* (derived from electrochemical measurements in 2-electrode setup) of $NiCo_2O_4$||N−rGO hybrid asymmetric supercapattery device with reported $NiCo_2O_4$ based symmetric/asymmetric devices.

Sl. No.	Positive Electrode Material	Negative Electrode Material	Asymmetric/Symmetric Device Name	Maximum Power Density (W kg^{-1})	Maximum Energy Density @ (power density)	Cyclic Stability (Cycle No.)	Reference No.
1	$NiCo_2O_4$ nanorods	$NiCo_2O_4$ nanorods	$NiCo_2O_4$||$NiCo_2O_4$	4003	12.6 W h kg^{-1}	94 % (2000)	s16
2	Co_3S_4 nanoneedles on $NiCo_2O_4$ nanosheets	Activated carbon (AC)	NC-9||AC	-	14 W h kg^{-1} (400 W kg^{-1})	84.7% (3000)	s36
3	$NiCo_2O_4$ nanosheets@hollow microrod arrays	Activated carbon (AC)	NSs@HMRAs||AC	7800	15.4 W h kg^{-1}	106 % (2500)	s37
4	MoS_2 nanowires/ $NiCo_2O_4$ nanosheets	Active carbon	MS/NCO||Active carbon	4500	18.4 W h kg^{-1} (1200 W kg^{-1})	98.2 % (8000)	s38
5	Mesoporous NiP@$NiCo_2O_4$ composite	Activated carbon (AC)	Ni-P@$NiCo_2O_4$||AC	5700	21 W h kg^{-1} (350 W kg^{-1})	78.3 % (8000)	s39
6	$NiCo_2O_4$ nanoneedle arrays	Activated carbon (WSs-2)	$NiCo_2O_4$||WSs-2	4254	21 W h kg^{-1} (424 W kg^{-1})	99.3 % (5000)	s40
7	$NiCo_2O_4$ nanosphere	Activated carbon (AC)	$NiCo_2O_4$||AC	-	21.5 W h kg^{-1} (750 W kg^{-1})	87.8 % (2000)	s41
8	Nickel cobalt oxide-reduced graphite oxide	Activated carbon (AC)	$NiCo_2O_4$-rGO||AC	12990	23.3 W h kg^{-1} (324 W kg^{-1})	83 % (2500)	s42
9	$NiCo_2O_4$ electrode	Activated carbon (AC)	NCO-9||AC	4860	23.6 W h kg^{-1} (585.5 W kg^{-1})	77 % (8000)	s43
10	Hexagonal $NiCo_2O_4$	Activated carbon (AC)	NCO||AC	1385	24.5 W h kg^{-1} (175 W kg^{-1})	90 % (2000)	s30
11	Crumpled graphene microspheres anchored with $NiCo_2O_4$ nanoparticles	Nitrogen-doped Crumpled graphene microspheres (N-CGM)	$NiCo_2O_4$/CGM ||N-CGM	7800	24.7 W h kg^{-1} (799.6 W kg^{-1})	85 % (50000)	s44
12	Carbon cloth/carbon fibers/$NiCo_2O_4$ composite	Carbon cloth/carbon fibers/$NiCo_2O_4$	CC/CFs/$NiCo_2O_4$|| CC/CFs/$NiCo_2O_4$	-	27.2 W h kg^{-1} (1460 W kg^{-1})	81% after 3000 Cycles	s45
13	$NiCo_2O_4$@ CNT/CNT multilayer electrode	Treated carbon cloth (TCC)	$NiCo_2O_4$@CNT/CNT|| TCC	2860	27.6 W h kg^{-1} (550 W kg^{-1})	95 % (5000)	s46

14	3D $NiCo_2O_4$@$ZnWO_4$ core-shell	$NiCo_2O_4$@ $ZnWO_4$ core-shell	$NiCo_2O_4$@$ZnWO_4$|| $NiCo_2O_4$@$ZnWO_4$	-	28.46 W h kg^{-1} (790 W kg^{-1})	97.5 % (5000)	s47
15	$NiCo_2O_4$ nanosheets	Activated carbon (AC)	$NiCo_2O_4$||AC	5346	30.75 W h kg^{-1} (900 W kg^{-1})	90.3 % (5000)	s26
16	Urchin-like $NiCo_2O_4$@3DNF framework	Nitrogen-doped porous carbon (NPC)	$NiCo_2O_4$@3DNF||NPC	3433.33	32.08 W h kg^{-1} (700.43 W kg^{-1})	100 % (8000)	s48
17	Hierarchical $NiCo_2O_4$/Ni_2P	Activated carbon (AC)	$NiCo_2O_4$/Ni_2P||AC	8000	40.7 W h kg^{-1} (800 W kg^{-1})	92 % (5000)	s14
18	Polypyrrole-decorated $NiCo_2O_4$ nanoneedles/carbon fiber papers	Nitrogen doped reduced graphene oxide (N-rGO)	PPyNiCo_2O_4@CFP|| N-rGO	3746.77	40.81 W h kg^{-1} (738.27 W kg^{-1})	88 % (5000)	s49
19	Nickel cobalt oxide-reduced graphene oxide composites	Reduced graphene oxide (rGO)	NCO/rGO|| rGO	8000	45.22 W h kg^{-1} (400 W kg^{-1})	81.7 % (10000)	s50
20	Urchin-shaped $NiCo_2O_4$	Activated Carbon (AC)	NiCoO||AC	6000	34.2 W h kg^{-1} (800 W kg^{-1})	90.0 % (1000)	s22
21	Ribbon-like $NiCo_2O_4$	Nitrogen doped reduced graphene oxide (N-rGO)	$NiCo_2O_4$||N-rGO	13003	30.55 W h kg^{-1} (5418 W kg^{-1})	94.3 % (10000)	This Work

References

(s1) Sonia, Y. K.; Paliwal, M. K.; Meher, S. K. The Rational Design of Hierarchical CoS_2/$CuCo_2S_4$ for Three-Dimensional All-Solid-State Hybrid Supercapacitors with High Energy Density, Rate Efficiency, and Operational stability. *Sustain. Energy Fuels* **2021**, *5*, 973−985.

(s2) Paliwal, M. K.; Meher, S. K. Hierarchically Organized Ultrathin NiO Nanofibers/Highly Defective-rGO Heteronanocomposite: An Advanced Electrode Material for Asymmetric Supercapacitors. *Adv. Mater. Interfaces* **2019**, *6*, 1900889 (1−13).

(s3) Paliwal, M. K.; Meher, S. K. Study of "Ni-Doping" and "Open-Pore Microstructure" as Physico-Electrochemical Stimuli Towards the Electrocatalytic Efficiency of Ni/NiO for the Oxygen Evolution Reaction. *New J. Chem.* **2020**, *44*, 17507−17517.

(s4) Chen, X.; Chen, D.; Guo; X.; Wang, R.; Zhang, H. Facile Growth of Caterpillar-like $NiCo_2S_4$ Nanocrystal Arrays on Nickle Foam for High-Performance Supercapacitors. *ACS Appl. Mater. Interfaces* **2017**, *9*, 18774−18781.

(s5) Wang, Y.; Zhang, M.; Li, Y.; Ma, T.; Liu, H.; Pan, D.; Wang, X.; Wang, A. Rational Design 3D Nitrogen Doped Graphene Supported Spatial Crosslinked Co_3O_4@$NiCo_2O_4$ on Nickel Foam for Binder-free Supercapacitor Electrodes. *Electrochim. Acta* **2018**, *290*, 12−20.

(s6) Paliwal, M. K.; Meher, S. K. Co_3O_4/$NiCo_2O_4$ Perforated Nanosheets for High-Energy-Density All-Solid-State Asymmetric Supercapacitors with Extended Cyclic Stability. *ACS Appl. Nano Mater.* **2020**, *3*, 4241−4252.

(s7) Pujol, O.; Bowen, P.; Stadelmann, P. A.; Hofmann, H. Growth and Self-assembly of Nanostructured CoC_2O_4,$2H_2O$ Particles. *J. Phys. Chem. B* **2004**, *108*, 13128−13136.

(s8) Rajeshkhanna, G.; Umeshbabu, E.; Rao, G. R. Charge Storage, Electrocatalytic and Sensing Activities of Nest-like Nanostructured Co_3O_4. *J. Colloid Interface Sci*. **2017**, *487*, 20−30.

(s9) Ogata, F.; Ueta, E.; Toda, M.; Otani, M.; Kawasaki, N. Adsorption of Phosphate ions From an Aqueous Solution by Calcined Nickel-Cobalt Binary Hydroxide. *Water Sci. Technol.* **2017**, *75*, 94−105.

(s10) Lawson, S.; Adebayo, B.; Robinson, C.; Al-Naddaf, Q.; Rownaghi, A. A.; Rezaei, F. The Effects of Cell Density and Intrinsic Porosity on Structural Properties and Adsorption Kinetics in 3D-Printed Zeolite Monoliths. *Chem. Eng. Sci.* **2020**, *218*, 115564 (1−13).

(s11) Yin, X.; Li, H.; Fu, Y.; Yuan, R.; Lu, J. Hierarchical Core-shell Structure of $NiCo_2O_4$ Nanosheets@HfC Nanowires Networks for High Performance Flexible Solid-state Hybrid Supercapacitor. *Chem. Eng. J.* **2020**, *392*, 124820 (1−11).

(s12) Feng, X.; Huang, Y; Li, C.; Chen, X.; Zhou, S.; Gao, X.; Chen, C. Controllable Synthesis of Porous $NiCo_2O_4$/NiO/Co_3O_4 Nanoflowers for Asymmetric All-solid-state Supercapacitors. *Chem. Eng. J.* **2019**, *368*, 51−60.

(s13) Zhou, Q.; Wang, X.; Liu, Y.; He, Y.; Gao, Y; Liu, J. High Rate Capabilities of $NiCo_2O_4$-Based Hierarchical Superstructures for Rechargeable Charge Storage. *J. Electrochem. Soc.* **2014**, *161*, A1922 (1−5).

(s14) Jia, H.; Li, Q.; Li, C.; Song, Y.; Zheng, H.; Zhao, J.; Zhang, W.; Liu, X.; Liu, Z.; Liu, Y. A. Novel Three-Dimensional Hierarchical $NiCo_2O_4$/Ni_2P Electrode for High Energy Asymmetric Supercapacitor. *Chem. Eng. J.* **2018**, *354*, 254−260.

(s15) Zou, R.; Xu, K.; Wang, T.; He, G.; Liu, Q.; Liu, X.; Zhang, Z.; Hu, J. Chain-like $NiCo_2O_4$ Nanowires With Different Exposed Reactive Planes for High-Performance Supercapacitors. *J. Mater. Chem. A* **2013**, *1*, 8560−8566.

(s16) Sethi, M.; Bhat, D. K. Facile Solvothermal Synthesis and High Supercapacitor Performance of $NiCo_2O_4$ Nanorods. *J. Alloys Compd*. **2019**, *781*, 1013−1020.

(s17) Yang, K.; Yan, Y.; Chen, W.; Zeng, D.; Ma, C.; Han, Y.; Yang, Y. Yolk-shell Bimetallic Metal-organic Frameworks Derived Multilayer Core-shells $NiCo_2O_4$/NiO Structure Spheres for High-performance Supercapacitor. *J. Electroanal. Chem.***2019**, *851*, 113445 (1−10).

(s18) Zhang, Y.; Wang, J.; Yu, L.; Wang, L.; Wan, P.; Wei, H.; Lin, L.; Hussain, S. Ni@$NiCo_2O_4$ Core/Shells Composite as Electrode Material for Supercapacitor. *Ceram. Int.* **2017**, *43*, 2057−2062.

(s19) Ouyang, Y.; Huang, R.; Xia, X.; Ye, H.; Jiao, X.; Wang, L.; Hao, Q. Hierarchical Structure Electrodes of NiO Ultrathin Nanosheets Anchored to $NiCo_2O_4$ on Carbon Cloth with Excellent Cycle Stability for Asymmetric Supercapacitors. *Chem. Eng. J.* **2019**, *355*, 416−427.

(s20) Wang, N.; Sun, B.; Zhao, P.; Yao, M.; Hu, W.; Komarneni, S. Electrodeposition Preparation of $NiCo_2O_4$ Mesoporous Film on Ultrafine Nickel Wire for Fexible Asymmetric Supercapacitors. *Chem. Eng. J.* **2018**, *345*, 31−38.

(s21) Han, S.; Lin, L.; Zhang, K.; Luo, L.; Peng, X; Hu, N. $ZnWO_4$ Nanoflakes Decorated $NiCo_2O_4$ Nanoneedle Arrays Grown on Carbon Cloth as Supercapacitor Electrodes. *Mater. Lett.* **2017**, *193*, 89−92.

(s22) Aparna, M. L.; Thomas, T.; Rao, G. R. Battery-like Supercapacitive Behavior of Urchin-Shaped $NiCo_2O_4$ and Comparison with $NiCo_2X_4$ (X= S, Se, Te). *J. Electrochem. Soc*. **2022**, *169*, 020515 (1−16).

(s23) Umeshbabu, E.; Rajeshkhanna, G.; Rao, G. R. Urchin and Sheaf-like $NiCo_2O_4$ Nanostructures: Synthesis and Electrochemical Energy Storage Application. *Int. J. Hydrogen Energy* **2014**, *39*, 15627−15638.

(s24) Deokate, R. J.; Kalubarme, R. S.; Park, C. J.; Lokhande, C. D. Simple Synthesis of $NiCo_2O_4$ Thin Films Using Spray Pyrolysis for Electrochemical Supercapacitor Application: A Novel Approach. *Electrochim. Acta* **2017**, *224*, 378−385.

(s25) Lv, Y.; Wang, H.; Xu, X.; Shi, J.; Liu, W; Wang, X. Balanced Mesoporous Nickle Cobaltite-Graphene and Doped Carbon Electrodes for High-Performance Asymmetric Supercapacitor. *Chem. Eng. J.* **2017**, *326*, 401–410.

(s26) Jabeen, N.; Xia, Q.; Yang, M.; Xia, H. Unique Core–Shell Nanorod Arrays With Polyaniline Deposited Into Mesoporous $NiCo_2O_4$ Support For High-Performance Supercapacitor Electrodes. *ACS Appl. Mater. Interfaces* **2016**, *8*, 6093–6100.

(s27) Guo, D.; Zhang, L.; Song, X.; Tan, L.; Ma, H.; Jiao, J.; Zhu, D; Li, F. $NiCo_2O_4$ Nanosheets Grown on Interconnected Honeycomb-like Porous Biomass Carbon for High Performance Asymmetric Supercapacitors. *New J. Chem.* **2018**, *42*, 8478–8484.

(s28) Chen, H.; Jiang, G.; Yu, W.; Liu, D.; Liu, Y.; Li, L.; Huang, Q. Electrospun Carbon Nanofiberic Coated with Ambutan-like $NiCo_2O_4$ Microspheres as Electrode Materials. *MRS Commun*. **2017**, *7*, 90–96.

(s29) Rajeshkhanna, G.; Umeshbabu, E.; Justin, P.; Rao, G. R. In situ Fabrication of porous Festuca Scoparia-like $Ni_{0.3}Co_{2.7}O_4$ Nanostructures on Ni-foam: An Efficient Electrode Material for Supercapacitor Applications. *Int. J. Hydrogen Energy* **2015**, *40*, 12303−12314.

(s30) Bhagwan, J.; Nagaraju, G.; Ramulu, B.; Sekhar, S. C.; Yu, J. S. Rapid Synthesis of Hexagonal $NiCo_2O_4$ Nanostructures for High-Performance Asymmetric Supercapacitors. *Electrochim. Acta* **2019,** *299*, 509−517.

(s31) Yao, D.; Ouyang, Y.; Jiao, X.; Ye, H.; Lei, W; Xia, X.; Lu, L.; Hao, Q. Hierarchical $NiO@NiCo_2O_4$ Core–Shell Nanosheet Arrays On Ni Foam for High-Performance Electrochemical Supercapacitors. *Ind. Eng. Chem. Res.* **2018,** *57*, 6246−6256.

(s32) Syedvali, P.; Rajeshkhanna, G.; Umeshbabu, E.; Kiran, G. U.; Rao, G. R.; Justin, P. In situ Fabrication of Graphene Decorated Microstructured Globe Artichokes of Partial Molar Nickel Cobaltite Anchored on a Ni Foam as a High-Performance Supercapacitor Electrode. *RSC Adv.* **2015**, *5*, 38407−38416.

(s33) Xiong, W.; Gao, Y.; Wu, X.; Hu, X.; Lan, D.; Chen, Y.; Pu, X.; Zeng, Y.; Su, J.; Zhu, Z. A. Composite of Macroporous Carbon with Honeycomb-Like Structure from Mollusc Shell and $NiCo_2O_4$ Nanowires for High-Performance Supercapacitor *ACS Appl. Mater. Interfaces* **2014,** *6*, 19416−19423.

(s34) Pan, C.; Liu, Z.; Li, W.; Zhuang, Y.; Wang, Q.; Chen, S. $NiCo_2O_4$@Polyaniline Nanotubes Heterostructure Anchored on Carbon Textiles with Enhanced Electrochemical Performance for Supercapacitor Application *J. Phys. Chem. C* **2019**, *123*, 25549−25558.

(s35) Feng, X.; Huang, Y.; Li.; C; Xiao, Y.; Chen, X.; Gao, X.; Chen, C. Construction Of Carnations-like Mn_3O_4@$NiCo_2O_4$@NiO Hierarchical Nanostructures for High-Performance Supercapacitors. *Electrochim. Acta* **2019,** *308*, 142−149.

(s36) Liu, Y.; Wen, S; Shi, W. Co_3S_4 Nanoneedles Decorated on $NiCo_2O_4$ Nanosheets for High-Performance Asymmetric Supercapacitors. *Mater. Lett.* **2018**, *214*, 194−197.

(s37) Lu, X. F.; Wu, D. J.; Li, R. Z.; Li, Q.; Ye, S. H. Tong, Y. X. and Li, G. R. Hierarchical $NiCo_2O_4$ Nanosheets@Hollow Microrod Arrays for High-Performance Asymmetric Supercapacitors. *J. Mater. Chem. A* **2014**, 2, 4706–4713.

(s38) Wen, S.; Liu, Y.; Zhu, F.; Shao, R; Xu, W. Hierarchical MoS_2 Nanowires/$NiCo_2O_4$ Nanosheets Supported on Ni Foam for High-Performance Asymmetric Supercapacitors. *Appl. Surf. Sci.* **2018**, *428*, 616–622.

(s39) Li, X.; Ding, R.; Yi, L.; Shi, W.; Xu, Q; Liu, E. Mesoporous Ni-P@ $NiCo_2O_4$ Composite Materials for High Performance Aqueous Asymmetric Supercapacitors. *Electrochim. Acta* **2016**, *222*, 1169−1175.

(s40) Wang, W.; Qi, J.; Sui, Y.; He, Y.; Meng, Q.; Wei, F.; Jin, Y. An Asymmetric Supercapacitor Based on Activated Porous Carbon Derived from Walnut Shells and $NiCo_2O_4$ Nanoneedle Arrays Electrodes. *J. Nanosci. Nanotechnol*. **2018**, *18*, 5600−5608.

(s41) Xu, K.; Yang, J.; Hu, J. Synthesis of Hollow $NiCo_2O_4$ Nanospheres with Large Specific Surface Area for Asymmetric Supercapacitors. *J. Colloid Interface Sci.* **2018**, *511*, 456−462.

(s42) Wang, X.; Liu, W. S.; Lu, X.; Lee, P. S. Dodecyl Sulfate-Induced Fast Faradic Process in Nickel Cobalt Oxide–Reduced Graphite Oxide Composite Material and its Application for Asymmetric Supercapacitor Device. *J. Mater. Chem.* **2012**, *22*, 23114−23119.

(s43) Sun, D.; Li, Y.; Cheng, X.; Shi, H.; Jaffer, S.; Wang, K.; Liu, X.; Lu, J.; Zhang, Y. Efficient Utilization of Oxygen-Vacancies-Enabled $NiCo_2O_4$ Electrode for High-Performance Asymmetric Supercapacitor. *Electrochim. Acta* **2018**, *279*, 269−278.

(s44) Yuan, R.; Chen, W.; Zhang, J.; Zhang, L.; Ren, H.; Miu, T.; Zhao, B. Crumpled Graphene Microspheres Anchored with $NiCo_2O_4$ Nanoparticles as Advanced Composite Electrode for Asymmetric Supercapacitor with Ultralong Cycling Life. *Dalton Trans.* **2022**. DOI: 10.1039/D2DT00195K.

(s45) Zhang, J. N.; Liu, P.; Jin, C.; Jin, L. N.; Bian, S. W.; Zhu, Q.; Wang, B. Flexible Three-Dimensional Carbon Cloth/Carbon Fibers/$NiCo_2O_4$ Composite Electrode Materials for High-Performance All-Solid-State Electrochemical Capacitors. *Electrochim. Acta* **2017,** *256*, 90−99.

(s46) Wu, P.; Cheng, S.; Yao, M.; Yang, L.; Zhu, Y.; Liu, P.; Xing, O.; Zhou, J.; Wang, M.; Luo, H.; Liu, M. A low-Cost, Self-Standing $NiCo_2O_4$@ CNT/CNT Multilayer Electrode for Flexible Asymmetric Solid-State Supercapacitors. *Adv. Funct. Mater.* **2017,** *27*, 1702160 (1−9).

(s47) Lin, L.; Li, L.; Hussain, S.; Zhao, S.; Wu, L.; Peng, X.; Hu, N. Hierarchical 3D $NiCo_2O_4$@$ZnWO_4$ Core-Shell Structures as Binder-Free Electrodes for All-Solid-State Supercapacitors. *Appl. Surf. Sci.* **2018**, *452*, 113−122.

(s48) Parveen, N.; Al-Jaafari, A. I.; Han, J. I. Robust Cyclic Stability and High-Rate Asymmetric Supercapacitor Based on Orange Peel-derived Nitrogen-Doped Porous Carbon and Intercrossed Interlinked Urchin-like $NiCo_2O_4$@3DNF framework. *Electrochim. Acta*, **2019**, *293*, 84−96.

(s49) Ko, T. H.; Lei, D.; Balasubramaniam, S.; Seo, M. K.; Chung, Y. S.; Kim, H. Y.; Kim, B. S. Polypyrrole-Decorated Hierarchical $NiCo_2O_4$ Nanoneedles/Carbon Fiber Papers for Flexible High-Performance Supercapacitor Applications. *Electrochim. Acta* **2017**, *247*, 524−534.

(s50) Budak, Ö.; Uğuz, Ö.; Koca, A. Simultaneous Electrochemical Deposition of Nickel Cobalt Oxide-reduced Graphene Oxide Composites for High Performance Asymmetric Supercapacitors. *J. Energy Storage* **2022**, *47*,103538 (1−15).